ISSN (Print) 1226-1750
ISSN (Online) 2233-6656
Journal of Magnetics 24(4), 628-633 (2019) https://doi.org/10.4283/JMAG.2019.24.4.628

Effect of Calcination Temperature on Magnetic Properties of MnZn Ferrites for High Frequency Applications

Lingfeng Wang, Guoli Lei, Chong Yan*, and Hongliang Ge

College of Materials Science and Engineering, China JiLiang University

(Received 9 August 2019, Received in final form 14 October 2019, Accepted 29 November 2019)

With the development of switching power supplies, miniaturization and high efficiency become hot research issues, and decreasing high-frequency losses is an effective method to achieve it. In this article, the effect of different calcination temperature on the power losses of MnZn ferrites at high frequency (500 kHz) over a broad temperature range is reported. The MnZn ferrites samples were prepared by ceramic process and the effect of calcination temperature was analyzed. The raw materials were calcined at 775 °C, 800 °C, 825 °C, 850 °C, 875 °C, 900 °C, 925 °C and 950 °C, and the regular fluctuations of particle size (as-calcined), density (as-sintered) and magnetic properties are presented in this work. It is shown that the samples calcined at 850 °C exhibit optimal microstructure and magnetic properties. The newly developed MnZn ferrites are characterized by sintered density of 4.61 g/cm^3, initial permeability of 1223 (10 kHz/0.1 mT/25 °C), saturation magnetic flux density of 488 mT (10 kHz/1200 A/m/25 °C) and power losses of 68 mW/cm^3 (500 kHz/50 mT/100 °C).

Keywords : calcination, pressing, MnZn ferrites, magnetic properties

1. Introduction

MnZn ferrites material ($Mn_xZn_{1-x}Fe_2O_4$) is one of the most important soft ferrites due to its high initial permeability, high saturation magnetization, high resistivity and low power losses. Besides, the excellent performances including controllable size and structural features, easy synthesis process and tunable electromagnetic properties [1-3] cater the needs of modern electric devices. Subsequently, MnZn ferrites are applied in various applications including inductors, transformers and absorbers, electronic or telecommunication equipment, defense and the automotive [4]. Consequently, it is crucial for the advance of modern electronic device to develop MnZn ferrites. High frequency, miniaturization and high efficiency are significant characteristics for the next generation electronic devices, which require magnetic components possessing excellent high-frequency performances [5-7]. Moreover, the preparation technics play a vital role in enhancing the magnetic properties of MnZn ferrites, however, calcination is an especially significant process. The purpose of the calcination is to form a small quantity of spinel structure and promote particle shrinkage, which is the important basis of sintering process. Furthermore, calcination is beneficial to achieve proper grain size, homogenize microstructure of as-sintered and finally improve its magnetic properties. In this work, different calcination temperatures were adopted to investigate the effect on magnetic properties and high-frequency performances.

2. Experimental details

2.1. Experimental procedure

The present work was carried out on MnZn ferrites with the chemical composition of Fe_2O_3:MnO:ZnO = 55.7:38.8:6.2 (mol%), which was fabricated with the conventional solid state reaction process shown in Fig. 1.

Fe_2O_3, Mn_3O_4, and ZnO were mixed for 1 h in deionized water and dried 16 h at 115 °C. The mixtures were calcined in air at various temperatures for 2 h (T_{CALC}: 775 °C to 950 °C with 25 °C intervals). The as-calcined samples with normal additives ($SiO_2 \cdot CaO \cdot ZrO_2$ and Nb_2O_5) were further wet-pulverized in a ball mill for 1.2 h, dried and subsequently roll-granulated with the addition of a plasticizer (10 wt.% aqueous solution of polyvinyl alcohol) through spraying method. Subsequently, the granulated samples were pressed twice under axial compaction (5

*Corresponding author: Tel: +86-157-5716-3474
Fax: +86-8-683-5731, e-mail: 13A0505069@cjlu.edu.cn

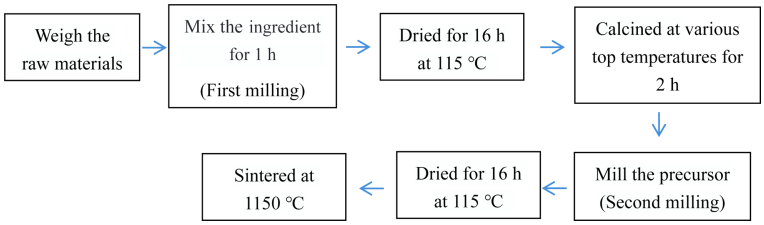

Fig. 1. (Color online) Schematic diagram of the experimental procedure for $Mn_xZn_{1-x}Fe_2O_4$ Synthesis.

MPa) to get toroidal samples (outer/inner diameter: 30 mm/17 mm/10 mm), and sintered at 1150 °C for 22 h using a specially constructed programmable kiln with firing schedules under equilibrium oxygen partial pressure conditions to ensure the stability of phases due to the equilibrium relation between oxygen partial pressure and temperature [8].

2.2. Characterize methods

The phases of the as-calcined and as-sintered samples were analyzed by X-ray diffraction. The XRD data were taken from 10° to 80° (0.02° step in 2θ) with Cu-Kα (λ = 1.54059 Å) radiation. Raman spectra were recorded by a laser Raman spectrophotometer (Renishaw in Via Reflex) equipped with a CCD camera with a laser of 785 nm over the range of 100-800 cm^{-1}. Furthermore, the powders (as-calcined) were characterized in terms of the distribution of particle size with laser diffraction method (Malvern Mastersizer-S). The density of as-sintered samples was measured by Archimedes' method. Polycrystalline microstructures of cross section of as-sintered samples were characterized by Scanning Electron Microscopy (SEM-Jeol 6300). The saturation magnetic flux density and power losses were measured by Iwatsu B-H analyzer (SY8232), and initial permeability was measured by Impedance analyzer (Agilent 4294A). Lakeshore Model 7404 vibrating sample magnetometer (VSM) was used for saturation magnetization measurement.

3. Results and Discussion

Fig. 2 shows the XRD patterns of powders calcined at different temperature (775 °C, 800 °C, 825 °C, 850 °C, 875 °C, 900 °C, 925 °C and 950 °C) and as-sintered samples. According to the analysis of the Fig. 2a, as-calcined samples mainly consist of α-Fe_2O_3 (JCPDS No.33-0664), Mn_2O_3 (JCPDS No.71-0636), and a small quantity of $ZnFe_2O_4$ (JCPDS No.65-3111). The valence of Zn ion is +2, thus, $ZnFe_2O_4$ is easily formed in air atmosphere. Obviously, there is no $MnFe_2O_4$ formed after calcination due to the O_2 in air. It is known that Mn_3O_4 contains two kinds of valence of +2 and +3, and the Mn^{2+} is easily

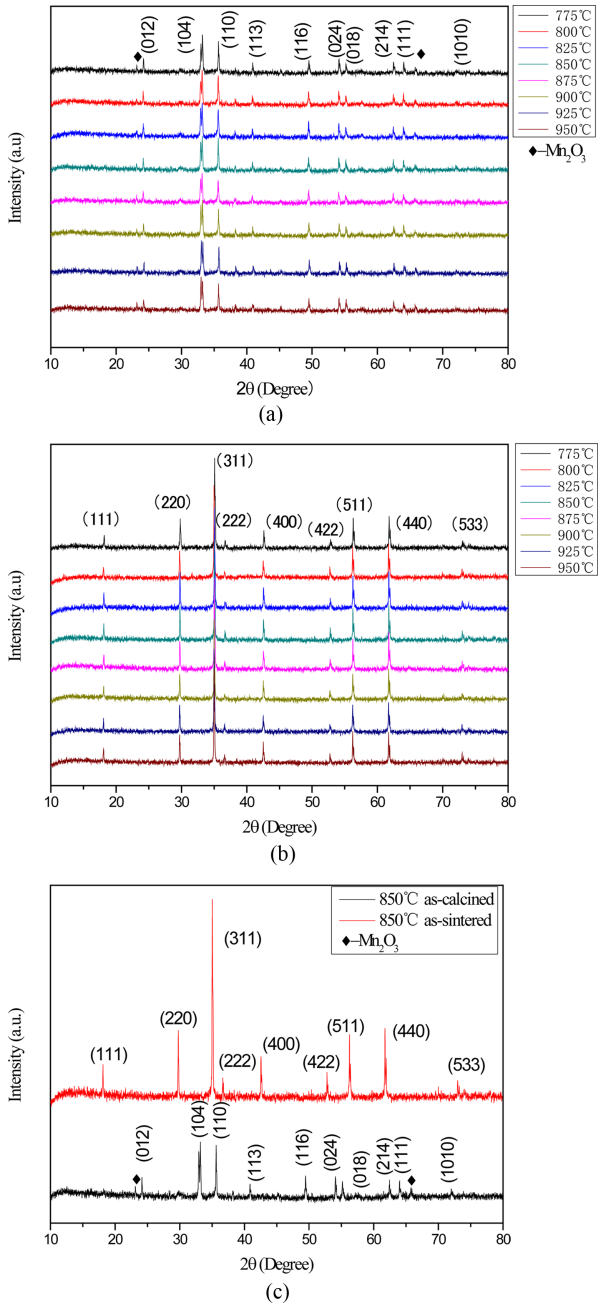

Fig. 2. (Color online) XRD patterns of MnZn ferrites, (a) calcined at 775 °C, 800 °C, 825 °C, 850 °C, 875 °C, 900 °C, 925 °C, and 950 °C, respectively; (b) as-sintered samples; (c) the comparison between as-calcined and as-sintered samples.

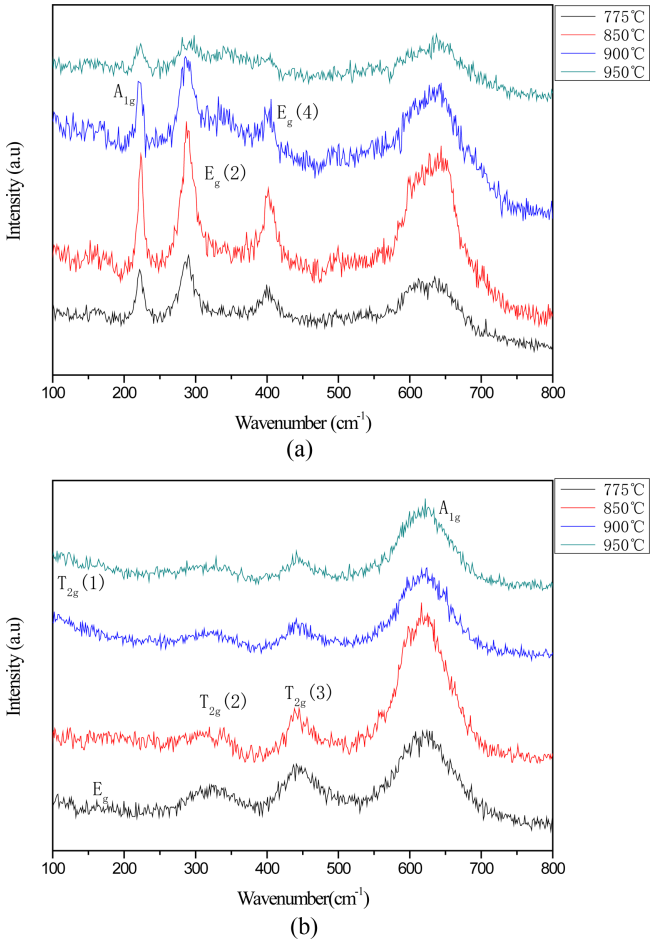

Fig. 3. (Color online) Raman spectra of MnZn ferrites, (a) as-calcined samples calcined at 775 °C, 850 °C, 900 °C and 950 °C, respectively; (b) as-sintered samples.

oxidized into Mn^{3+} by O_2. Consequently, the peak of $MnFe_2O_4$ is not shown in XRD patterns of as-calcined samples. $MnFe_2O_4$ phase is formed after sintering in protection atmosphere of N_2 shown as spinel phase in Fig. 2b. The comparison results of as-calcined and as-sintered samples are presented in Fig. 2c, which confirms the formation of pure spinel phase.

Besides, the Raman spectra were recorded at 300 K in the frequency range from 100 to 800 cm^{-1} for further confirmation of the results of XRD analysis in Fig. 3 [4, 9, 10]. Fig. 3 shows the Raman spectra of as-calcined (775 °C, 850 °C, 900 °C, and 950 °C) and as-sintered samples. The Raman spectra demonstrate that α-Fe_2O_3 peaks (A_{1g} = 224 cm^{-1}, E_g (2) = 290 cm^{-1} and E_g (4) = 400 cm^{-1}) are detected in the as-calcined samples in Fig. 3a. In addition, three distinct characteristic peaks (T_{2g} (2) = 325 cm^{-1}, T_{2g} (3) = 443 cm^{-1} and A_{1g} = 622 cm^{-1}) are observed in all spectra, and E_g and T_{2g} (1) at the range from 100 to 200 cm^{-1} are ambiguous. However, it is still

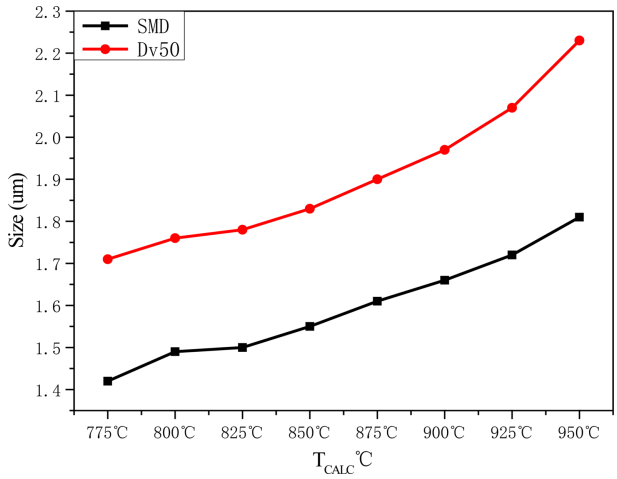

Fig. 4. (Color online) Particle size distribution of as-calcined samples.

illustrated that pure cubic spinel structure of AB_2O_4 is formed in as-sintered samples. These results are well corroborated with XRD data.

Fig. 4 shows the distribution of particle size of as-calcined samples. The particle size increases significantly with calcination temperature (T_{CALC}) according to the variety of Dv50 and SMD (Fig. 4). Meanwhile, The SEM micrographs, shown in Fig. 5, demonstrate that the microstructure of as-sintered samples is improved at proper T_{CALC}. It is observed that the initial increase of T_{CLC} from 775 °C to 850 °C yields the gradual expansion of the grains of the as-sintered samples and remarkable reduction of intergranular pores, which also confirms that the low T_{CALC} leads to low reactivity. Below 850 °C, the microstructure becomes more uniform with the increase of T_{CALC}, shown in Fig. 5. Consequently, the uniform microstructure leads to density improved, which exhibits an increase of respective sintered density (D_S) from 4.61 g/cm^3 to 4.69 g/cm^3 shown in Fig. 6. Further increase of T_{CALC} (above 850 °C) favors the appearance of exaggerated grain growth leading to pores formed as shown in Fig. 5c and d. The further increase of T_{CALC} trends to make the increase of concentration of Zn-rich ferrite phases formed in the as-calcined powders. Subsequently, the Zn-rich ferrite phases grow rapidly at the expense of other phases, however, Zn trends to evaporate during sintering [11]. Consequently, intergranular pores increase and D_S decreases, as shown in Fig. 6. Besides, nucleation and growth would possibly release O_2. As the chemical equation shown [12]:

$$2Fe_e^{3+} + 3/4V_c + O^{2-} \rightleftharpoons 2Fe^{2+} + 1/2O_2 \quad (1)$$

Fe ions would combine with cation vacancies (V_c) in Fe-rich MnZn ferrites, which releases O_2 and makes

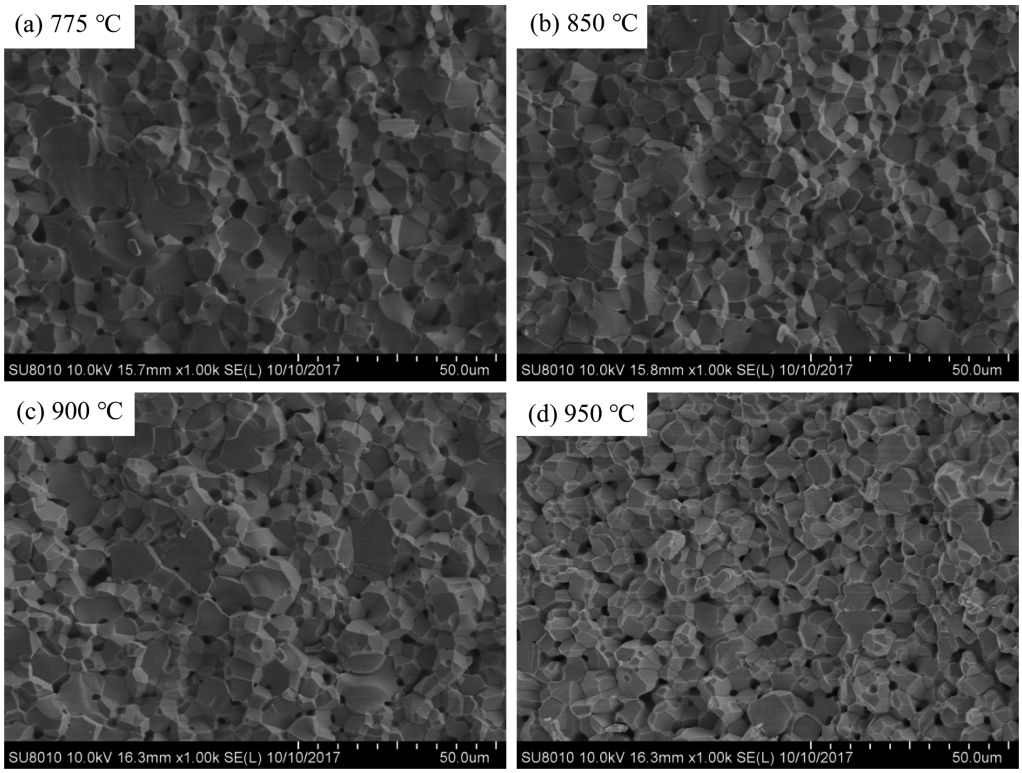

Fig. 5. SEM images of as-sintered samples calcined at (a) 775 ℃, (b) 850 ℃, (c) 900 ℃, and (d) 950 ℃, respectively.

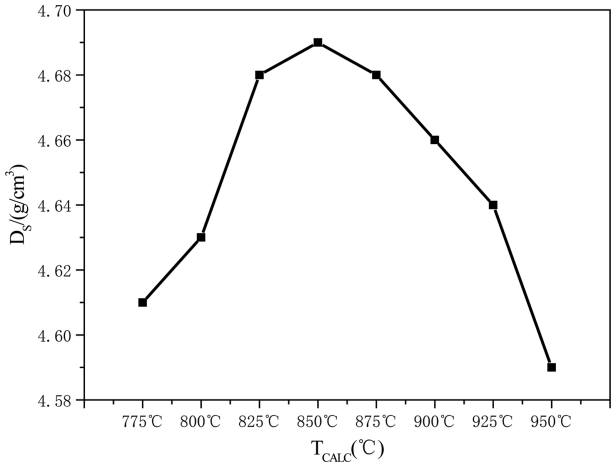

Fig. 6. Sintered density (D_s) of as-sintered samples calcined at 775 ℃, 800 ℃, 825 ℃, 850 ℃, 875 ℃, 900 ℃, 925 ℃ and 950 ℃, respectively.

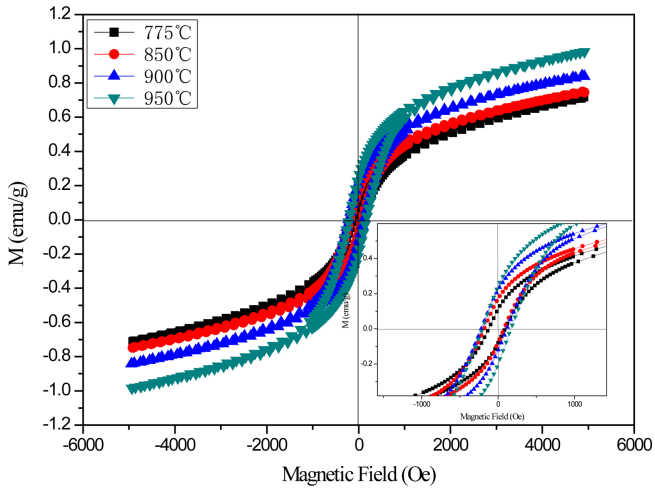

Fig. 7. (Color online) Magnetic hysteresis loops (300 K) of as-calcined samples. The inset graph illustrates the variation of residual magnetization in magnetic hysteresis loop.

porosity increased. High T_{CALC} makes (1) accelerated and pores are formed indirectly in bulk sample shown in Fig. 5. Therefore, optimal T_{CALC} is necessary for homogeneous microstructure.

Fig. 7 shows magnetization hysteresis loops of as-calcined samples (T_{CALC} = 775 ℃, 850 ℃, 900 ℃, and 950 ℃). It is suggested that magnetization hysteresis loops are unsaturated and the coercivity (H_c) of as-calcined samples is large, however, MnZn ferrites are paramagnetic-like [13]. Consequently, the spinel structure is formed incompletely in as-calcined samples and α-Fe_2O_3 is the main composition in as-calcined samples, which accords with XRD analysis (Fig. 2). As ref [13] reported, α-Fe_2O_3 would cause magnetization hysteresis loop unsaturated. According to Fig. 7, the saturation magnetization (M_S) and residual magnetization (M_r) further increase with the

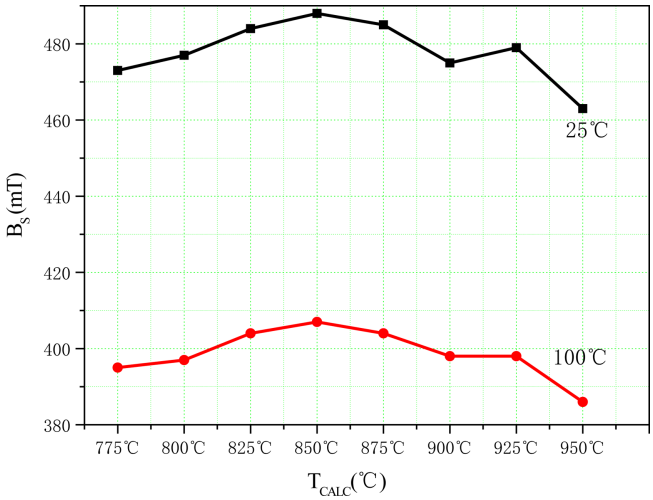

Fig. 8. (Color online) Saturation magnetic flux density B_s of as-sinterd samples for different calcination temperature, measured at 25 °C and 100 °C.

T_{CALC}. This is partly attributed to the increase of particle size.

Initial permeability (μ_i), saturation magnetic flux density (B_S), and power losses (P_{cv}) of the prepared ferrites are measured respectively, which is the crucial parameters as a high-frequency inductive power converter. The B_S of the samples measured at a magnetic field of 1200 A/m and 25 °C is shown in Fig. 8. According to the theory of ferrimagnetism, there are differences about resultant net magnetization between tetrahedral (A) and octahedral (B) sublattice in spinel ferrite [14]. Thus, due to the preserved magnetic structure and distribution of cationic in the lattice of the materials, B_S should be mainly dependent on density (D_S). B_S (T) is calculated by Eq. (2) and Eq. (3) [15]:

$$B_S(T) = B_S(0) \times (1 - T/T_C)^r \times D/D_1 \quad (2)$$

$$B_S(0) = M_S(0) \times n \times \mu_B \times N_a \times D_a/M \quad (3)$$

Here B_S (T) is the magnetic flux density at T K, B_S (0) is the magnetic flux density at 0 K, ρ is the density of the ferrites core, D is the actual density of ferrite, D_1 is the theoretical density of ferrite, T_C is the Curie temperature (K), r is a constant obtained by experiment, M_S (0) is the magnetization at 0 K, n is the Bohr magneton number, N_a is the Advogadro's number, M is the molecular weight, and D_a is the average density of ferrites. From Eq. (2), B_S (T) is proportional to D under certain test condition, which accords to Fig. 6. It is noticed that the samples calcined at 850 °C obtain the highest D_S of 4.69 g/cm^3 and exhibit the highest B_S of 488 mT (25 °C) and 407 mT (100 °C). The B_S decreases with further increase of T_{CALC}, which is attributed to the decrease of density.

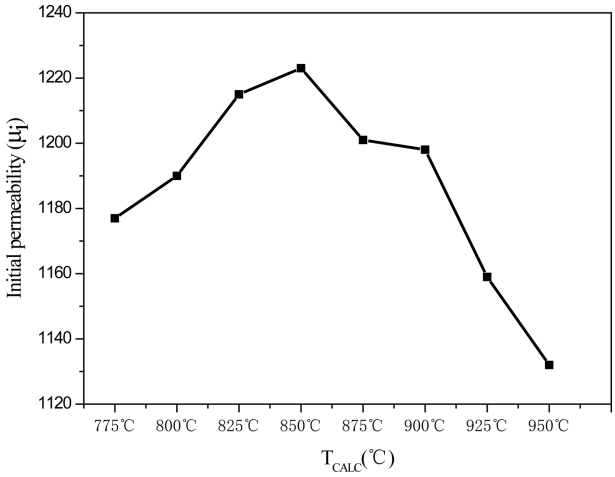

Fig. 9. Initial permeability (μ_i) of as-sintered samples.

The initial permeability (μ_i) and power losses (P_{cv}) of the toroids were measured under condition of 10 kHz/0.1 mT/25 °C and 500 kHz/50 mT/100 °C, respectively. The μ_i of as-sintered samples increases when T_{CALC} increases from 775 °C to 850 °C, and decreases with further increase of T_{CALC} (see Fig. 9). The maximum initial permeability is 1223 obtained at 850 °C due to the excellent microstructure with less pores (see Fig. 4) and high density (see Fig. 6). Since the initial permeability is proportional to the square of saturation magnetization and reversely proportional to anisotropy constant (K) and magnetostriction coefficient (λ), as described in Eq. (4) [16]:

$$\mu_i = M_S^2/(aK + b\lambda\sigma) \quad (4)$$

Where μ_i is initial permeability, M_S is saturation magnetization, K is magnetocrystalline anisotropy constant, λ is magnetostriction coefficient, σ is inner stress and a,b are constants. It is concluded that the increase of the

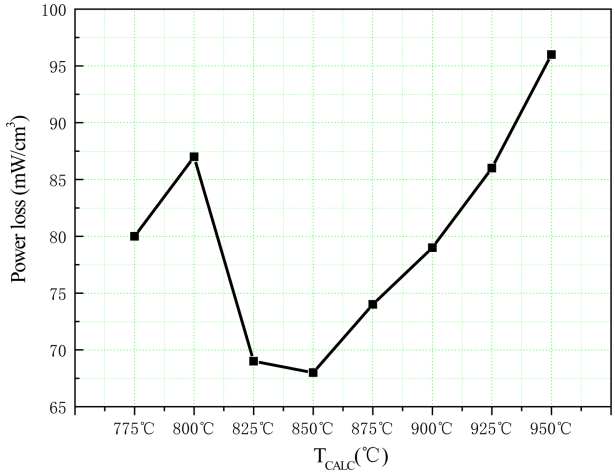

Fig. 10. (Color online) Power losses at 500 kHz, 50 mT, 100 °C.

initial permeability of as-calcined samples below 850 °C is attributed to the increase of M_S and decrease of λ and K [17].

Fig. 10 shows the power losses measured at 500 kHz/ 50 mT/100 °C. Eddy current loss is the dominant part for core losses, is usually defined as [6]:

$$P_e = K_e f^2 B^2 / \rho \quad (5)$$

K_e represents the coefficient of eddy current losses. B represents the magnetic flux density, *f* represents the frequency and ρ represents the resistivity of the core. It is evident that $P_e \propto 1/\rho$. According to Verwey's hopping mechanism [18], the electrical conduction of ferrite originates from electron hopping between the ions of the same element but of different valence states present at the octahedral (B-site). Electron hops between Fe^{3+} and Fe^{2+} ions ($F_e^{3+} + e^- \rightleftharpoons F_e^{2+}$), which is hindered by additives to enhance the resistivity. Consequently, the minimum of P_{cv} (100 °C) is obtained at 850 °C due to the homogeneous distribution of grain size and low porosity. Besides, uniform distribution of grain size is capable to make ρ increased, and decrease P_e. These samples possess excellent high-temperature performance (low P_{cv} at 100 °C), which stems from the value of magnetocrystalline anisotropy closing to zero at this temperature (100 °C) [16]. Then, the optimized power losses of 68 mW/cm^3 (500 kHz/50 mT/ 100 °C) are obtained.

4. Conclusions

In the present study, traditional ceramics technology is adopted due to its ease of operation and low cost. Subsequently, the effect of calcination temperature (T_{CALC}) in the range of 775 °C-950 °C on compaction and magnetic properties of MnZn ferrites ceramics is investigated. The positive correlation between the T_{CALC} and the distribution of particle size is established and explained. According to our research, the samples calcined at 850 °C exhibit the optimal microstructure and best magnetic properties. The newly developed MnZn ferrites exhibit initial permeability of 1223, and power losses of 68 mW/cm^3 (500 kHz/50 mT/100 °C). Therefore, it is concluded that an optimal combination of compaction and magnetic properties is attained when T_{CALC} is 850 °C. Consequently, it is necessary for MnZn ferrites manufacture to choose an appropriate T_{CALC} because of its sensitivity of process.

Acknowledgement

This work was supported by Rogers Corporation.

References

[1] H. Shokkrollahi and K. Janghorban, J. Mater. Sci. Eng. B **141**, 91 (2007).
[2] G. Kogias and V. Zaspalis, J. Physics Procedia. **75**, 1286 (2015).
[3] F. Fiorillo, C. Beatrice, O. Bottauscio, A. Manzin, and M. Chiampi, J. Appl. Phys. Lett. **89**, 122513 (2006).
[4] S. Thota, S C. Kashyap, S. Sharma, and V. R. Reddy, J. Physics and Chemistry of Solids **91**, 136 (2016).
[5] B. Sun, F. G. Chen, W. D. Yang, H. Q. Shen, and D. Xie, J. Magn. Magn. Mater. **349**, 180 (2014).
[6] D. Stoppels, J. Magn. Magn. Mater. **160**, 323 (1996).
[7] V. Loyau, G. -Y. Wang, M. Lo Bue, and F. Mazaleyrat, J. Applied Physics **111**, 053928 (2012).
[8] R. Morineau and M. Paulus, J. IEEE Trans. Magn. **5**, 1312 (1975).
[9] J. Kreisel, G. Lucazeau, and H. Vincent, J. Solid State Chem. **137**, 127 (1998).
[10] W. B. White and B. A. DeAngelis, J. Spectrochim. Acta. **23**, 985 (1967).
[11] P. Sainamthip and V. R. W. Amarakoon, J. Am Ceram Soc. **71**, 644 (1988).
[12] A. Broese van Groenou, P. F. Bongers, and J. A. L. Stuyts, Mater. Sci. Eng. **3**, 317 (1968).
[13] Z. H. Jing, S. H. Wu, S. M. Zhang, S. M. Zhang, and W. P. Huang, J. Materials Research Bulletin. **39**, 2057 (2004).
[14] J. Smit and H. P. J. Wijn, Ferrites: physical properties of ferrimagnetic oxides in relation to their technical applications, M. Philips' Technical Library, Eindhoven, The Netherlands, 1959.
[15] T. Hiraga, K. Okutani, and T. Ojima, Ferrite, M. Maruzen Co. Ltd, Japan, Toky, 1986.
[16] A. Goldman, Handbook of Modern Ferromagnetic Materials, M. Kluwer Academic Press, 1999.
[17] A. Goldman, Modern Ferrite Technology Second Edition, M. Pittsburgh, PA, USA, 2006.
[18] E. J. W. Verwey and J. H. De Boer, J. Rec. Tray. Chim. Pays. Bas. **531**, 55 (1936).